Published in final edited form as:

Wiley Interdiscip Rev Nanomed Nanobiotechnol. 2019 March ; 11(2): e1541. doi:10.1002/wnan.1541.

Nanoparticles to mediate X-ray-induced photodynamic therapy and Cherenkov radiation photodynamic therapy

Benjamin Cline[1], **Ian Delahunty**[1], and **Jin Xie**[1,2]

[1]Department of Chemistry, University of Georgia, Athens, Georgia

[2]Bio-Imaging Research Center, University of Georgia, Athens, Georgia

Abstract

Photodynamic therapy (PDT) has emerged as an attractive option for cancer treatment. However, conventional PDT is activated by light that has poor tissue penetration depths, limiting its applicability in the clinic. Recently the idea of using X-ray sources to activate PDT and overcome the shallow penetration issue has garnered significant interest. This can be achieved by external beam irradiation and using a nanoparticle scintillator as transducer. Alternatively, research on exploiting Cherenkov radiation from radioisotopes to activate PDT has also begun to flourish. In either approach, the most auspicious success is achieved using nanoparticles as either a scintillator or a photosensitizer to mediate energy transfer and radical production. Both X-ray induced PDT (X-PDT) and Cherenkov radiation PDT (CR-PDT) contain a significant radiation therapy (RT) component and are essentially PDT and RT combination. Unlike the conventional combination, however, in X-PDT and CR-PDT, one energy source simultaneously activates both processes, making the combination always in synchronism and the synergy potential maximized. While still in early stage of development, X-PDT and CR-PDT address important issues in the clinic and hold great potential in translation.

This article is categorized under:

Therapeutic Approaches and Drug Discovery > Nanomedicine for Oncologic Disease

Keywords

Cherenkov radiation; nanoparticles; photodynamic therapy; radiation therapy; scintillation; X-ray induced photodynamic therapy

1 | INTRODUCTION

The national cancer institute estimates that 1,685,210 new cases of cancer are diagnosed in the United States every year, with 595,690 people dying from the disease. The mainstay treatment options are surgery, radiation, chemotherapy, and endocrine therapy (Urruticoechea et al., 2010). However, the U.S. Surveillance Epidemiology and End Results

Correspondence Jin Xie, Department of Chemistry, University of Georgia, Athens, GA 30602. jin.xie@uga.edu.

CONFLICT OF INTEREST

The authors have declared no conflicts of interest for this article.

data suggest that there have been only a 14% decline in age-adjusted mortality rates over the past 35 years. As such, researchers have long been searching for new treatment options (Noone et al., 2018). One promising modality is photodynamic therapy or PDT. For cancer therapy, photosensitizers are delivered to tumors, and are stimulated by light to generate reactive oxygen species (ROS), most importantly singlet oxygen ($^1O_2$), to damage tumor cells or induce tissue ischemia (Huang et al., 2008). PDT is associated with a low level of systemic toxicity because photosensitizers are usually pharmaceutically inactive in the dark and photo-irradiation is given only to tumor areas in the procedure. Further, PDT can be applied repeatedly without cumulative toxicity or incurring resistance (Agostinis et al., 2011). Moreover, multiple studies showed that local PDT treatment can stimulate systemic antitumor immunity, leading to suppression of distant tumors or metastases (Gollnick, Vaughan, & Henderson, 2002; Korbelik, 2011; Oseroff, 2006; van Duijnhoven, Aalbers, Rovers, Terpstra, & Kuppen, 2003).

Despite these promises, the uses of PDT in the clinic have been limited. One major problem has been the challenge of delivering sufficient light to tumors in internal organs. Visible or near-infrared light has a penetration depth of less than 1 cm through body tissues, limiting PDT treatment to diseases that are close to the skin (Hopper, 2000; Kalka, Merk, & Mukhtar, 2000). One possibility to circumvent the limitation is to deliver light through an optical fiber. This allows PDT to target certain internal organs. For instance, PDT is approved to treat lung, esophagus, mouth and skin cancer in the United States and gastric cancer in the Japan (Huang, 2005). Very recently, a clinical trial in Europe showed that PDT reduced the prevalence of low-risk prostate cancer by 35% over 2 years compared to those who received observation only (Emberton, 2016). Still, the light delivery is often limited by tumor size and location.

It has been postulated that if light could be produced adjacent to photosensitizers, penetration depth would no longer be an issue. One exciting approach is X-ray-induced PDT or X-PDT. X-PDT exploits a nanoparticle scintillator to down-convert external X-ray photons to visible light photons; the latter in turn actives near-by photosensitizers to trigger PDT. Unlike visible or Near-infared (NIR) light, X-rays afford superior tissue penetration and can potentially expand the scope of PDT in clinical applications. Another emerging approach is Cherenkov radiation-induced PDT or CR-PDT. Cherenkov radiation occurs when a particle travels faster than the speed of light through a medium, which is seen with multiple radioisotopes (Shaffer, Pratt, & Grimm, 2017) (Hoogendam et al., 2016; Phillips et al., 2014; Pratt, Shaffer, & Grimm, 2016). Research shows that Cherenkov radiation from medical radioisotopes can activate photosensitizer to produce ROS (Kotagiri et al., 2018). Both external-beam radiation and internal irradiation are widely utilized for cancer treatment, underscoring the clinical relevance and prospects of X-PDT and CR-PDT. In this review article, we attempt to summarize recent progress on X-PDT and CR-PDT to elucidate the mechanism behind the efficacy of the therapies and to provide insight and inspiration for its future advancement (Figure 1).

2 | X-RAY LUMINESCENCE AND CHERENKOV IRRADIATION

When exposed to a light source, a photosensitizer undergoes either a type 1 or type 2 photochemical reaction. In a type 1 reaction, the excited state photosensitizer transfers an electron to surrounding biomolecules, producing superoxide radical anions, such as highly reactive hydroxyl radicals (Maisch et al., 2007). For a type 2 reaction, an excited triple-state photosensitizer transfers energy directly to molecular oxygen, forming $^1O_2$. $^1O_2$ is extremely reactive due to the pairing of two electrons into one of the antibonding orbitals (Marchetti & Karsili, 2016). This allows $^1O_2$ to directly destroy tumor cells through apoptosis or necrosis and as such is often used as an indicator for PDT lethality.

An effective cytotoxic dose of $^1O_2$ has been reported to be approximately 5×10^7–2×10^9 molecules per cell (Niedre, Secord, Patterson, & Wilson, 2003). Thus, efficient luminescence generated through scintillation or Cherenkov radiation is crucial. Although both X-Ray and Cherenkov luminescence have long been known, it is only recently that their potential in biomedical imaging and therapy has been intensively studied. Therefore, achieving high photon yield in biological environments is an area of active interest.

2.1 | X-ray luminescence

Scintillating materials have long been used in the fields of detection, dosimetry, and diagnosis (Dujardin et al., 2010). The scintillation process is an extreme form of optical down conversion with three steps in the basic mechanism. First, incident irradiation ionizes the material, forming holes in the highest energy shells. More specifically, incident irradiation excites outer shell electrons, triggering a series of radiative electron decays, followed by the emission of secondary X-rays, nonradiative decays (e.g., Auger electrons), and electron-electron inelastic scattering (e.g., Compton scattering). This process occurs on the order of 10^{-15}–10^{-13} s and requires 2–7 times the energy threshold to make an electron hole pair. Second, there is a gradual release of the absorbed energy until the ionization threshold is reached. At this point, the energy has dissipated to the point where it can no longer propagate further ionizations; instead, it promotes interband transitions, leading to the creation of electron hole pairs. Electron–photon relaxation and interband transitions promote thermalization. Charge carriers can return to the diffuse band (as in semiconductors), be trapped in defects or impurities (as in dopants), or self-trapped to its own structure or form excitons, these processes take 10^{-12}–10^{-11} s. In the third and final step, the excited luminescent center returns to the ground state by photon emission or nonradiative suppression. The radiative process is usually short (10^{-9}–10^{-3} s) for pair recombination, exciton emission, or electronic recombination, but may take several minutes if the process is highly prohibitive (Cebim, Oliveira, Krauser, & Davolos, 2017).

For bulk scintillators, elemental composition and structure are the major parameters affecting luminescence efficiency. The ideal scintillator should have high efficiency converting absorbed high-energy photons into relaxed electrons and holes, transferring relaxed electron–hole pairs toward the emitting center, and emitting center luminescence yield. The photoabsorption cross sections of the inner-shell electrons are much larger than those of the outer-shell electrons. As such, high-Z elements, which have more inner shell electrons, are more efficient in capturing X-ray photons (Band, Kharitonov, &

Trzhaskovskaya, 1979). For this reason, the majority of bulk scintillators are high-Z elements doped with rare earth metals. Where structure is concerned, the fewer defects present in a material the fewer nonradiative processes occur, leading to higher the emission intensity. Minimizing the number of defects in a bulk scintillation material is based on many aspects of the synthetic method, but one of the most important parameters is reaction temperature. Many materials show an exponential increase in emission intensity with annealing, which improves crystallinity and thus reduces defects (Lempicki, Wojtowicz, & Berman, 1993). Phase is another parameter that influences the optical properties. For instance, a hexagonal phase $NaGdF_4:Eu^{3+}$ scintillator was found to be 25% more intense than its cubic structure counterpart (Sudheendra et al., 2014). Both coordination number and covalence degree of the dopant at the crystallographic site play a critical role in bulk material scintillation defining the luminescent properties from efficiency to wavelength.

For X-PDT, nanoparticles, rather than bulk scintillators, are used due to their bio-applicability, surface functionality and passive tumor targeting (Davis & Shin, 2008). While the aforementioned principles still apply, nanoparticle scintillators have their own sets of rules for synthesis and luminescent properties. Nanomaterials have expanded the possibilities for X-ray luminescence uses in high-energy physics and medical imaging, providing a large portfolio of compositions including composite films, vitroceramics, thin films, coordination compounds, metal–organic frameworks (MOFs), and organic–inorganic hybrid materials (Cooper, Bekah, & Nadeau, 2014; Hamieh, Dorkenoo, Taupier, Henry, & Halley, 2017; Pereira, Martin, Levinta, & Dujardin, 2015; Vistovskyy et al., 2014; Vistovskyy et al., 2016; Wahid, Pokhrel, & Mao, 2017). Even pure metals and semiconductors, which usually do not function as X-ray scintillators, may function as such if formed into nanoparticles (Brus, 1984; Paillard et al., 1999; Yuan et al., 2013).

Size reduction to the nanoscale has a plethora of effects to the scintillation properties. Key among these is the increased importance of the particle surface conditions. Due to the high surface to volume ratio inherent in nanoparticles, a significant proportion of scintillation activator sites are present on the surface of the particle and are exposed to surface conditions. Additionally, given the small size of the nanomaterial and the high mobility of excitonic excitations, surface activators are more frequently stimulated than in their bulk counterparts (Dujardin et al., 2010). This means that all surface interactions such as defects, coatings, and media interaction all impact luminosity to a larger degree than in bulk materials. Furthermore, materials size reduction may cause surface strengths to induce an additional pressure leading to crystal field fluctuations. This causes energy levels to be distributed randomly, decreasing the probability of direct energy transfer, and consequently increasing the chance of a radiative transition.

In practice, there have been some mixed results with scintillator size reduction for doped nanoparticles. For instance, severe quenching was observed in $Gd_2O_3:Eu^{3+}$nanoparticles under high-energy excitation, while enhancement has been observed with $YSO:Ce^{3+}$ nanoparticles (Ledoux et al., 2004; Muenchausen et al., 2008). Jung et al. (2014) analyzed the radioluminescence emission properties in the range 300–400 nm of 15 nanoscintillators, and found that for many standard X-ray phosphors, the quantum efficiency of nano-sized powders is far less than that of micron-sized powders. They theorized this to be due to

luminescence quenching from defects found on the surface (e.g., dangling bonds, absorbed species) and from disorder in the lattice surrounding the activator ion. However, it has also been observed that nanoscintillators have some improved properties over single crystals. The rise time is shortened in borates, and 90-nm sized powders of YAG:Eu^{3+} scintillators exhibited maximum luminous output, which was four times that of the single large crystal (Klassen et al., 2005). For semiconductors, on the other hand, the reduction of size leads to a violation of the momentum conservation law (i.e., quantum confinement) and as such luminescence yield increases as the size decreases (Brus, 1984; Paillard et al., 1999).

The additional disorder applied by surface strengths poses a challenge when optimizing nanoparticle scintillators. Bottom up synthetic methods often produce particles of poor crystallinity, and efforts to anneal the particles often result in irreversible aggregation (Chen et al., 2017). Top-down synthetic methods have the advantage of better crystallinity and therefore higher luminescence, but have suboptimal size control. The majority of classical X-PDT studies so far have been conducted with nanoparticles made from a top-down approach. Meanwhile, efforts are being made to develop synthetic approaches that enable nanoparticles to undergo annealing without causing aggregation (Gaspar, Mazali, & Sigoli, 2010).

There are two major classes of nanoscintillators, namely doped scintillator and semi-conductor. Of doped scintillators, lanthanides have been the most widely explored (Sudheendra et al., 2014). This is largely attributed to their high material density, high atomic number, and strong luminescence intensity. In particular, nanoparticles of the formulation $ALnF_4$ (A = Alkaline, Ln = Lanthanide) have a band gap in the range of 9–10 eV and are very suitable for X-ray down-conversion. Semiconductor nanoscintillators made from ZnO, Si nanocrystals, porous Si, CuBr, PbS, CdSe, and CdS have also been explored (Alivisatos, 1996; G Ledoux, Gong, Huisken, Guillois, & Reynaud, 2002; Nanda, Kruis, Fissan, & Behera, 2004; Rama Krishna & Friesner, 1991; Viswanatha et al., 2004). The size of these particles is often kept as small as possible to maximize quantum entanglement effects (Table 1).

2.2 | Cherenkov radiation

The Cherenkov effect is observed when a charged particle travels faster than the speed of light through a medium (Cherenkov, 1960). In tissue (refractive index ~1.40), a β particle needs an energy >250 keV to exceed the speed of light and emit visible photons. Almost all medical isotopes pass this threshold (Gonzales et al., 2014). Although originally detected in 1958, the first biologically relevant use of Cherenkov radiation was documented by Robertson et al. (2009) in mice with ^{18}F and ^{13}N. The researchers proposed a unique bimodal imaging system where the same agent is detectable by both optical imaging and positron emission tomography. Later, Thorek, Ogirala, Beattie, and Grimm (2013) studied Cherenkov radiation interacting with quantum dots for secondary Cherenkov-induced fluorescence imaging. Since that time several studies have reported that Cherenkov radiation can be exploited to activate PDT (Hartl, Hirschberg, Marcu, & Cherry, 2016; Kamkaew et al., 2016; Kotagiri, Sudlow, Akers, & Achilefu, 2015).

Using Cherenkov radiation to induce PDT offers several potential advantages. For one it could eliminate the need for external beam irradiation and potentially minimize healthy tissue exposure. Moreover, many radiopharmaceuticals are able to accumulate selectively in tumors after systematic injection (Packer, 1984). This could allow CR-PDT to target multiple tumor loci with high selectivity. A major downside of CR-PDT, however, is the extremely low fluence rates of Cherenkov radiation. While there is no accepted universal lower fluence limit for PDT, a number of in vitro and in vivo studies have found that a decrease in cytotoxicity occurs when fluence rate is below 5.5 mW/cm^2 (Bellnier & Lin, 1985; Henderson, Busch, & Snyder, 2006). Monte Carlo simulations have determined the flux rates for radionuclides to be on the order of 0.01–1 nW/cm^2 per MBq g^{-1}. For most treatments this would put fluence several orders of magnitude below where researchers have observed decreased phototoxicity (Glaser, Zhang, Andreozzi, Gladstone, & Pogue, 2015).

3 | X-RAY-INDUCED PDT

In this section, we explore classic X-PDT, defined as having a nanoscintilator localized in close proximity to a photosensitizer with matching excitation wavelength. We introduce the origin of the technique as well as the related theoretical modeling and simulations. We discuss the importance of scintillator materials and nanoparticle surface modification on X-PDT efficiency.

3.1 | Origins and design considerations

The idea of using X-ray energy to facilitate PDT has been floating around since the mid 80s. In 1989 it was proposed that tissues irradiated by X-rays could produce red light and excite haematoporphyrin derivatives for PDT (Bistolfi, 2000). The idea of using scintillator nanoparticles to stimulate photosensitizers was first proposed by Chen and Zhang (2006). The group explored two classes of nanoparticle scintillators: doped nanoparticles ($LaF_3:Ce^{3+}$, $LuF_3:Ce^{3+,}$ $CaF_2:Mn^{2+}$, $CaF_2:Eu^{2+}$, $BaFBr:Eu^{2+}$, $BaFBr:Mn^{2+}$, and $CaPO_4:Mn^{2+}$) and semiconductor nanoparticles (CdS, ZnO, ZnS, and TiO_2). From these CdS was selected and conjugated to porphyrin through EDC/NHS coupling. The group demonstrated the emission and absorption spectrum overlap as well as the quenching of the CdS scintillator spectrum after conjugation with the porphyrin. However, in this pioneer work, no studies were performed to determine ROS generation or toxicity under X-ray (Figure 2a).

Following this conceptual study, several theoretical models were generated to estimate the capability of X-PDT. Results from initial simulations were not encouraging. One such study by Morgan, Kramer-Marek, Smith, Camphausen, and Capala (2009) drew on the contemporary literature, combining results for nanoparticle targeting of tumor tissues and $^1O_2$ measurements in PDT to determine the expected lethality of the technique. The authors attempted to model, based on literature consensus, whether lethal levels of $^1O_2$ could be obtained without lethal levels of radiation. Using LaF_3 as a case study the authors concluded that for energies above 300 keV, an excess of 60 Gy is required to achieve enough $^1O_2$ per cell for a killing dose. Common radiation therapy (RT) involves a total radiation dose of 50–70 Gy, at energies around 6–20 MeV (Majumder, Choudhury, Das, Kundu, & Mitra, 2013).

As such X-PDT would only be useful it treatments where low energies were applicable and at higher energies provide no significant advantage over RT. Further, from the literature the authors determined 5% volume fraction for the nanoparticle uptake was a difficult but attainable goal. From this they determined that at above 300 keV, where the absorption of LaF_3 is <20x that of the cell, the cell absorbs more radiation than the scintillating nanoparticles. The authors acknowledged some limitations within their model, for instance the difficulty accounting for potential radiosensitizing effects (a considerable effect seen in later studies) and that full cellular internalization is not required for a cytotoxic effect. Additionally, the total radiation dose is not as important as the localized damage delivered to key cellular processes. Cancerous cells with X-PDT and radiosensitizing nanoparticles at energies above 300 keV will see a significant increase in lethality compared to RT at the same dose (Takahashi & Misawa, 2007). Still, the simulation work raised good questions on the practicality of X-PDT as an effective treatment modality.

Further simulation studies proved more promising. Bulin et al. (2015) determined that the Morgan paper underestimated the energy deposition in nanoparticles. Specifically, scintillation includes both primary and secondary excitations, and their migration distances may exceed nanoparticle's size, leading to increased energy deposition. Clement, Deng, Camilleri, Wilson, and Goldys (2016) created a more optimistic X-PDT model and supported it by quantifying experimental $^1O_2$ quantum yield and in vitro studies. The authors synthesized 9-nm CeF_3 particles via a co-precipitation method and electrostatically adsorbed verteporfin to the particle surface. For their particles, they determined that 60 Gy of 6 MeV and 30 keV corresponds to $(1.2 \pm 0.7) \times 10^8$ and $(2.0 \pm 0.1) \times 10^9$ $^1O_2$/cell. The exact number of $^1O_2$ molecules required for lethality varies considerably and the value in the literature is between 5×10^7 and 2×10^9 molecules per cell (Morgan et al., 2009; Niedre et al., 2003). The authors assumed that 5×10^7 $^1O_2$ molecules per cell result in 1/e clonogenic surviving fraction. Thus, 1.2×10^8 to 2.0×10^9 $^1O_2$ molecules per cell would correspond to ~10% and negligible surviving fraction, respectively. To validate their conclusions the authors performed an in vitro X-PDT experiment with pancreatic cancer cell lines. At 6 MeV and 6 Gy 32% of the cells were killed compared to a negligible fraction with X-ray alone.

The X-PDT efficiency is dependent on a number of factors, notably the X-ray luminescence intensity of the nanoscintillators, the $^1O_2$ quantum yield of the photosensitizers, and the spectrum overlap between the two. Moreover, how the photosensitizer binds to nanoparticle surface may largely affect the X-PDT efficiency. The three methods most commonly used are electrostatic interactions, pore loading, and covalent bonding (Chen et al., 2015; Chen, Wang, et al., 2017; Clement et al., 2016; Elmenoufy, Tang, Hu, Xu, & Yang, 2015). Though there is no hard rule for minimum distance between nanoscintilator and photosensitizer but, given the poor light penetration in tissues it can be assumed that X-PDT efficiency is proportional to the distance between the two. Some researchers maintain that the distance between the two should be less than 10 nm. This would allow for radiationless Forster resonance energy transfer to occur, minimizing energy loss during transition and potentially improving radical production efficiency (Chen & Zhang, 2006; Elmenoufy et al., 2015). So far, there have been few studies to systematically examine the impact of the loading methods on X-PDT efficiency.

Another factor worth investigation is the contribution of X-ray luminescence and fluorescence on cell lethality. The scintillation process may generate UV or other ionizing irradiation. It has been proposed that UVC alone can be harnessed to damage cells and cancerous tissues (Justel & Feldmann, 2007). How to differentiate these effects from the PDT contribution remains a challenge. On the other hand, it is fair to admit that X-PDT is intrinsically a complicated process and the cell death a result of multiple factors. Likely, these understudied factors account for the discrepancy between the theoretical models and the real practice.

Furthermore, the intratumoral or intracellular distribution of nanoparticles are hardly homogeneous and this distribution profile may largely affect cytotoxicity. Given the short penetration of radicals, the damage is likely focused on membrane or organelles enriched with nanoparticles. Rossi et al. (2015) observed very high X-PDT efficacy with SiC/SiO_x core/shell nanowires in killing adenocarcinomic alveolar basal epithelial cells, and they attributed this to a large degree to the almost complete cell uptake of the nanowires. Mitochondria targeted X-Ray ROS production has been shown in vivo to induce mitochondrial collapse and significantly more cellular apoptosis than X-rays alone or the untargeted nanoparticles (Li et al., 2018). The ability to alter the energy deposition profile could contribute to the cell killing mechanism of X-PDT.

3.2 | Classic X-PDT

The Chen and Zhang (2006) pioneered the exploration with X-PDT. They took $LaF_3:Ce^{3+}$, $LuF_3:Ce^{3+,}$ $CaF_2:Mn^{2+}$, $CaF_2:Eu^{2+}$, BaFBr:Eu^{2+}, BaFBr:Mn^{2+}, and $CaPO_4:Mn^{2+}$, CdS, ZnO, ZnS, and TiO_2 and compared photosensitizers of matching absorbance wavelengths, such as photofrin, fullerenes, and TiO_2. In this initial study they demonstrated that for CdS nanoparticles conjugated with tretrakis (o-aminophenyl) porphyrin under X-ray the emission of the nanoparticles decreased while the fluorescence of tretrakis (o-aminophenyl) porphyrin increased (Figure 2b).

Progress in nanoparticle synthesis and fabrication has led to more comprehensive studies. Among all the scintillators tested rare earth materials, for instance terbium including compounds, have been most widely explored. This is likely due to terbium's favorable emission spectrum, which consists of four peaks centered at 488 nm (intraconfigurational transition 4f8 −4f8 5D4 → 7F6), 545 nm (5D4 → 7F5), 588 nm (5D4 → 7F4), and 625 nm (5D4 → 7F3). Elmenoufy et al. (2015) covalently conjugated LaF_3:Tb nanoparticles with a Rose Bengal photosensitizer and the same group demonstrated a similar formulation but with the Rose Bengal loaded into silica pores instead (Tang, Hu, Elmenoufy, & Yang, 2015). For both formulations the group evaluated $^1O_2$ generation in solution as the measure of X-PDT efficiency. Bulin et al. (2013) synthesized Tb_2O_3 nanoparticles and linked porphyrin to the particle surface. With this approach, Bulin et al. evaluated the energetics of the energy transfer between the scintillator and photosensitizer as well as X-Ray-induced $^1O_2$ generation. Chen, Wang, et al. (2017) synthesized terbium nanoparticles conjugated to meso-tetra(4-carboxyphenyl)porphyrin for X-PDT brain cancer therapy and have shown its efficacy with cell studies. The therapy showed a significant cell viability drop (≈50%) on 9 L glioma cells at 80 keV compared to X-Ray alone.

Other lanthanide materials have also been studied, many with cellular studies. For instance Zou et al. (2014) demonstrated $LaF_3:Ce^{3+}$ nanoparticles (emission at 520 nm) conjugated with PPIX induced oxidative stress, mitochondrial damage, and DNA fragmentation in PC3 cells under X-ray irradiation. Clement et al. (2016) conjugated CeF_3 nanoparticles with Verteporfin and assessed both $^1O_2$ generation and lethality against Panc1 cells at low and high energies. Kaščáková et al. (2015) synthesized lanthanide-based micelles (GdEuC12) and incorporated Hypercin into them. They observed $^1O_2$ production and cytotoxicity with the formulation upon X-ray irradiation. Recently a novel core dual shell system proposed by Hsu, Lin, and Chang (2018) used lanthanides to enable X-PDT and X-ray fluorescence without resonance quenching. The group measured the $^1O_2$ generation and in vitro toxicity of the $NaLuF_4$:Gd(35%),Eu(15%)@$NaLuF_4$:Gd(40%)@$NaLuF_4$:Gd(35%),Tb(15%) nanoparticles. Recently, a series of new nanoparticle formulations have been proposed for X-PDT. These include $Ce_{0.85}Tb_{0.15}F_3$ nanoparticles in a CTAB chlorin e6 shell, $12CaO{\cdot}7Al_2O_3:Tb^{3+}$ nanocages, $(Y_{1-x}Pr_x)_3Al_5O_{12}$ nanocrystals, and $GdVO_4:Eu^{3+}$ nanoparticles conjugated to methylene blue (Cooper, Capobianco, & Seuntjens, 2018; Jung et al., 2014; Li et al., 2017; Losytskyy et al., 2016, 2017; Song et al., 2018; Yefimova et al., 2017). However, none of these particles have yet moved beyond energetics analysis.

Some nonlanthanide materials have also shown potential in facilitating X-PDT. Rossi et al. (2015) synthesized SiC/SiO_x core/shell nanowires and evaluated these materials as X-PDT agents (Figure 3a). The nanowire cores are grown on silicon through chemical vapor deposition using a vapor–liquid–solid process (Fabbri et al., 2012). The nanowires show negligible cytotoxcicity in the dark and 545 nm fluoresce under X-ray. The nanowires are then functionalized with azide groups and covalently coupled with a porphyrin derivative through click chemistry. 12 days after 6 MeV and 2 Gy irradiation the authors observed a 75% reduction in A549 cells compared to the control (Figure 3f). Another interesting nonlanthanide X-PDT particle was proposed by Losytskyy et al. (2016). The particle is a polystyrene-based scintillator conjugated to chlorin e6 and showed encouraging energetics for X-PDT.

A further advantage of the dual nature of X-PDT is the radioenhancement effect that can be provided by nanoparticles. In these direct conversion particles, the absorption of X-ray energy excites electrons into states above the conduction band edge and excited electron hole pairs are subsequently trapped at the particle surface. The electron holes then interact with water to form hydroxyl radicals, and the electrons react with O_2 to form superoxide/peroxy radicals (Takahashi & Misawa, 2007; Townley, Kim, & Dobson, 2012). Ma, Zou, and Chen (2014) synthesized copper-cysteamine complex (Cu-Cy) nanoparticles and investigated their capacity to produce $^1O_2$ under X-ray irradiation. The authors examined the X-PDT efficacy in vitro via live/dead assays and observed extensive lethality at 2 Gy (90 keV). Under the same principle, a series of other X-PDT nanoparticles have been tested, such as octahedral molybdenum cluster compound $(n\text{-}Bu4N)_2[Mo6I8(OOC\text{-}1\text{-}adamantane)_6]$, colloidal GdSe and Gd_2O_3 nanoparticles, alginate-coated iron nanoparticles, ZnS:Ag CeF_3, and a series of Cd-based quantum dots to name a few (Generalov, Kuan, Chen, Kristensen, & Juzenas, 2015; Kim et al., 2009; Kirakci et al., 2015; Sheng, Li, Weiss, & Wang, 2012; Takahashi & Misawa, 2007; Yang et al., 2008). The authors consider these to have an advantage above conventional X-PDT nanoparticles as it saves the energy transfer

step, potentially leading to a higher $^1O_2$ quantum yield. However, it is debatable if these therapies technically count as X-PDT since no separate photosensitizers are involved.

Despite the extensive in vitro studies, it is not until recently that X-PDT was tested in vivo. Encouraged by the success of the Cu-Cy nanoparticle in vitro, the Chen group pursued in vivo experiments with subcutaneous mouse model MCF-7 cells (Ma, Zou, & Chen, 2014). When the particles were injected intratumorally without X-ray the tumors saw an increase of 250% over 13 days where as those exposed to 5 Gy of 90 keV X-rays and particles saw a reduction in tumor size by 25%. Townley et al. (2012) performed in vivo analysis with silica coated TiO_2:Gd^{3+} nanoparticles in rodent A549 xenograft models. Compared to X-rays alone, the nanoparticle and X-ray (200 keV) doubled the treatment efficacy and even provided significant tumor reduction after multiple rechallenging. Interestingly, the authors observed better outcomes with nanoparticles at 1 mg/mL than at 5 mg/ML, the mechanism behind this effect remains unknown.

Our group developed an integrated nanosystem containing a $SrAl_2O_4$:Eu^{2+}(SAO) nanoscintillator core, a mesoporous silica coating, and a photosensitizer merocyanine 540 (MC540) loaded into the silica layer for in vivo analysis (Figure 4a) (Chen et al., 2015). SAO emits green X-ray luminescence (~520 nm), which well matches the excitation wavelengths of MC540. MC540–SAO nanoparticles efficiently mediated X-PDT, killing U87MG (Chen et al., 2015) and H1299 cells (G. D. Wang et al., 2016), both cell lines that are refractory to RT. The treatment remained effective when cancer cells were lain under 4.5-cm thick pork tissues (Wang et al., 2016), which is not possible with conventional PDT. When injected directly into subcutaneous tumors (Chen et al., 2015) or implanted along with cancer cells to the lung, MC540–SAO nanoparticles in conjugation with external beam irradiation led to much greater tumor suppression than radiation alone (Figure 4f).

Zhang et al. (2015) evaluated $LiYF_4$:Ce@ZnO core/shell nanoparticles as a X-PDT agent in vivo with xenograft HeLa tumor models. In this nanosystem, $LiYF_4$:Ce is the scintillator and ZnO the photosensitizer. The group was able to completely inhibit tumor growth after 15 days compared to a marginal tumor suppression from RT alone. The group postulated that the $LiYF_4$:Ce@ZnO nanoparticles produced hydroxyl radicals through the type 1 PDT pathway, which is less oxygen-dependent than the type 2 pathway that is preferred in conventional PDT. This study evaluated X-PDT performance under low oxygen conditions, and illustrated that ROS production remained relatively stable when oxygen content was reduced (from 21% to 2%) whereas X-Ray alone saw a significant decrease in ROS generation. However, more studies are needed to understand the impact of oxygen level change on X-PDT efficiency.

Another interesting avenue of research is the use of nanoscale metal–organic frameworks (nMOFs) as X-PDT nanoconjugates. MOFs are a class of hybrid materials formed by the self-assembly of metal ions or clusters and organic polydentate bridging ligands. This nanoplatform offers a unique approach to bring together scintillators and photosensitizers at close proximity and with good control. Several groups have explored chlorin- and porphyrin-based MOFs (Lu, He, & Lin, 2015; Park, Jiang, Feng, Mao, & Zhou, 2016). Liu et al. (2016) developed a nMOF capable of radio sensitization and PDT and demonstrated its

effect in vivo. The MOFs were composed of Hf cores to serve as radiosensitizers and tetrakis (4-carboxyphenyl) porphyrin (TCPP) bridging ligands to serve as the photosensitizer. This concept was further advanced in a publication by Lan et al. (2017) in which the authors developed nanoscale organic layers for X-PDT therapy. At the nanoscale size the authors speculated that due to ROSs short lifetime, a significant portion of ROSs generated would not diffuse out of the 3D nMOF structure. Therefore, in an attempt to improve the X-PDT efficacy, the group reduced the dimensionality and created 2D nanoscale metal–organic layers (nMOLs) instead.

In a prior publication the Lin group had demonstrated that a Hf-based nMOF could absorb X-rays and transfer that energy to coordinated anthracene-based ligands which would then generate luminesce in the visible spectrum (Wang et al., 2014). Seeing the potential, Lan et al. (2017) combined an anthracene-based Hf nMOL with two photosensitizers, Ir[2,2′-bipyridine (2-phenylpyridine)$_2$]$^+$ and [Ru(2,2′-bipyridine)$_3$]^2 to induce X-PDT. When tested in vitro, the nMOLs were capable of dramatically reducing the viability of two colon cancer cell lines, CT26 and MC38, through X-PDT so the group moved to in vivo evaluation. When 0.5 nmol of nMOLs were intratumorally injected and treated with 5 Gy radiation, the researchers were able to reduce the tumor volume by 83.6% for CT26 tumors and with 10 Gy reduce MC38 tumor volume by 90.1% (Figure 5e).

3.3 | X-PDT by persistent luminescence

While using an X-ray to stimulate PDT has many advantages, concerns remain about the dose of radiation being delivered to healthy tissues. A possible solution is to exploit nanoscintillators that emit persistent luminescence. Unlike fluorescence, which has a lifetime of nanoseconds, persistent luminescence from some phosphors can endure for minutes or even hours after the end of excitation (Chen et al., 2014). This would allow for X-PDT to remain active in the absence of external irradiation, which may lead to reduced X-ray exposure for normal tissues and with minimal concerns about enhanced particle toxicity as the persistent luminescence will expire before most particles are cleared from the tumor sites (Liu et al., 2013).

For persistent luminescence X-PDT, the nanoparticle design is no different from classical X-PDT save for the scintillator used. Homayoni et al. (2016) explored $Sr_2MgSi_2O_7$:Eu^{2+},Dy^{3+}, a well-known afterglow material, as a X-PDT agent. $Sr_2MgSi_2O_7$:Eu^{2+},Dy^{3+} nanoparticles have four X-ray luminescence emission peaks at 408, 480, 580, and 660 nm. Only the 480-nm emission, which comes from the 5d to 4f transition of seven coordination site Eu^{2+}, is persistent (Fei, Chang, & Mao, 2005). The authors observed particle luminescence for up to 5,000 seconds after the end of X-ray irradiation. They then coated the particles in silica and conjugated to the surface both PpIX and folic acid. However, the study did not evaluate if the afterglow component was significant enough to mediate PDT and kill cancer cells.

Ma et al. (2014) prepared TBrRh123-loaded ZnS:Cu,Co nanoparticles and investigated their potential in persistent luminescent X-PDT. The authors measured two components to the decay lifetime. A short-lived component at 510 nm and the long-lived component at 546 nm, which lasted more than 10 minutes. They attributed the afterglow at 546 nm to the Cu^{2+} ions shifted from the normal wavelength of 525 nm by crystal defects. The authors showed that

the nanoparticles were efficiently internalized by PC3 cancer cells and, with 2 Gy irradiation, reduced cell viability by 40%. The authors claimed that this lethality was comparable to classical X-PDT mediated by MTCP-LaF_3:Tb nanoparticles at 13.2 Gy and they attributed the enhanced sensitizing effect to the persistent luminescence property of ZnS:Cu,Co nanoparticles, although the hypothesis would be difficult to prove. Recently Song et al. (2018) doped $ZnGa_2O_4$:Cr nanoparticles with W(VI) improving the scintillators afterglow capabilities. They then evaluated its energetics for use in X-PDT. Beyond providing another X-PDT scintillating option this study is of interest as it may provide insight on improving the afterglow properties of other nanoscintillators.

We recently synthesized $LiGa_5O_8$:Cr nanoparticles and tested their potential to mediate X-PDT. $LiGa_5O_8$:Cr affords long and intense afterglow after X-ray irradiation (Chen et al., 2017). More uniquely, the luminescence is centered in the near-infrared spectrum window (~720 nm). When coated with mesoporous silica and loaded with 2,3-naphthalocyanine (NC), a photosensitizer, the resulting nanoparticles can function as a theranostic agent with both imaging and X-PDT capabilities. in vitro studies showed NS-$LiGa_5O_8$:Cr@$mSiO_2$ nanoparticles still produce $^1O_2$ after the end of X-ray irradiation, and the resulting radicals were sufficient to kill H1299 cells. We conjugated to the nanoparticle surface Cetuximab, an anti-EGFR antibody, and intravenously injected the conjugates to mouse orthotopic lung cancer models. The nanoparticles were able to selectively accumulate in lung tumors, and the nanoparticles' afterglow was detected by IVIS in a “bioluminescence” imaging mode (i.e., without excitation). With 6 Gy external irradiation, the nanoparticle mediated X-PDT and induced efficient tumor suppression.

While persistent luminescence may allow for continued production of radicals after the end of X-ray irradiation, the intensity of the luminescence often diminishes rapidly, and so then does cytotoxicity. Moreover, an extended energy endurance does not necessarily guarantee an increased energy deposition in tumors. There is no proof that persistent luminescence is beneficial regarding energy transfer efficiency and photosensitizer activation, although it is speculated that persistent luminescence is associated with low speed of oxygen consumption, and may avoid anoxia seen with PDT. Overall, X-PDT with afterglow is an interesting concept, but relevant studies are few and far between. Further research is needed to elucidate how much afterglow X-PDT contributes to therapy and why.

4 | CHERENKOV RADIATION-INDUCED PDT

4.1 | CR-PDT stimulated by radioisotopes

Cherenkov luminescence (CL)-based optical imaging has long been investigated and approved for medical use (Ciarrocchi & Belcari, 2017). Recently, several groups have exploited Cherenkov radiation as an energy source to activate PDT. One strategy is to pair a radionuclide and a photosensitizer in a nanoparticle package. For instance, Kamkaew et al. (2016) encapsulated oxophilic zirconium-89 (^{89}Zr) and chlorin e6 into a mesoporous silica nanoparticle. Cherenkov emission peaks in the UV but still shows strong blue emission. Since one absorption peak of chlorin e6 is ~400 nm, the two are a good pair for CR-PDT. Chlorin e6 is barely released from the nanoparticles (only 9% after 2 days), which is beneficial as ^{89}Zr has a relatively long half-life (78.4 hr). in vitro studies with 4 T1 cells

found a high level of DNA double-strand breaks with the CR-PDT nanoparticles relative to ^{89}Zr alone. Intratumoral injection of the CR-PDT nanoparticles led to complete tumor eradication in 14 days at a sublethal (15 MBq) radiation dose (Figure 6c). One potential safety concern, however, is that many nanoparticles were found in the liver on Day 14, with significant amounts of the radioisotopes and photosensitizers remaining active (≈12% ^{89}Zr and 44% Ce6).

Instead of delivering radioisotopes and photosensitizers using the same nanoplatform, some groups have explored a colocalization approach, where radionuclides and photosensitizers are injected separately but co-enriched in cancer cells. This means that the therapy is only active when the components are in the tumor, limiting concerns about persistent toxicity as seen with previous CR-PDT particles. This approach exploits the fact that many clinically approved radiotracers accumulate in cancer cells with high efficiency and selectivity (Packer, 1984). Kotagiri et al. (2015) tested 2-deoxy-2′-(^{18}F)fluoro-D-glucose (^{18}F-FDG) as the Cherenkov source and TiO_2 nanoparticles as the photosensitizer. ^{18}F-FDG is the mostly commonly used positron emission tomography tracer and as a glucose analog it accumulates in tissues with high metabolism rates, such as tumors (Kelloff et al., 2005). Meanwhile, transferrin was conjugated to TiO_2 nanoparticles to facilitate nanoparticle tumor targeting. in vitro studies showed that incubation with ^{18}F-FDG and TiO_2 nanoparticles led to breached cell membrane integrity and vacuolated cytosol, features associated with necrosis while the separate components induced minimal toxicity. Intravenous injection of ^{18}F-FDG and transferrin TiO_2 nanoparticles then showed significant tumor suppression in vivo. With the tumor volume reduced to one-eighth of the controls on day 15. Another ^{18}F-FDG co-localization CR-PDT study by the same group used titanocene-loaded nanomicelles as the photo sensitizer (Kotagiri et al., 2018). These micelles were conjugated with LLP2A for VLA-4 ($\alpha_4\beta_1$ integrin) targeting. The latter is a plasma membrane protein overexpressed in ≥95% of the multiple myeloma human cell line MM1.S. When tested in disseminated multiple myeloma mouse models ^{18}F-FDG plus the titanocene nanomicelles led to selective and effective tumor suppression.

Compared with X-PDT, CR-PDT has certain advantages. For instance, CR-PDT can potentially target multiple metastases, which is challenging for classic X-PDT. The co-localization approach is also unique. Both radiotracers and photosensitizers can be rendered to be tumor targeting, making the treatment highly selective as the PDT activation can only occur when the two components meet within a cancer cell. A main concern with CR-PDT, however, is its low efficacy (Pratx & Kapp, 2018). The number of photons generated by radionuclides is several orders of magnitude lower than those during external irradiation, not to mention the loss of energy during conversion (Glaser et al., 2015). As mentioned above, Monte-Carlo simulations showed that the flux rates for radionuclides to be on the order of 0.01–1 nW/cm^2 per MBq g^{-1}. This amount of photons is deemed insufficient to produce effective phototoxicity (Glaser et al., 2015). If this is the case then how CR-PDT induces cancer cell death? It is likely the damage induced by the radionuclides improves on the lethality that could be expected from PDT alone, perhaps inducing a synergistic effect, as discussed in detail later. (Williams, DeNardo, & Meredith, 2008).

A recent study by Pratt, Shaffer, Zhang, Drain, and Grimm (2018), however, offers an approach to eliminate the low luminescence yields of CR-PDT. The group examined the impacts of decay and secondary products from radionuclides on nanoscintillators. By mixing sub-CL β emitting radionuclides with scintillating nanoparticles they were able to achieve a luminescence of nearly 2,500 times what was observed with the nuclide alone. Although γ-emitting radionuclides also showed a significant increase in luminescence when in proximity to a nanoscintillator the group discovered that β-scintillation induced radiance enhancement fourfold that of γ. They attributed this to the ability of β particles to interact with matter through multiple pathways including CL, electron excitation, ionization, bremsstrahlung, and annihilation (β^+ only). Γ particles on the other hand interact with matter through the photoelectric or Compton effects, coherent scattering, or pair production. In addition to the scintillation observed the group also generated characteristic X-ray energies through an L shell electron occupying the vacancy of a previously ejected K shell electron which they used as an additional imaging step. The authors concluded nanoparticles in proximity to either β- or γ-emitting radionuclides exhibit enhanced total photon flux and emit at discrete wavelengths in systems with luminescent metal ions.

4.2 | CR-PDT stimulated by external irradiation

Cherenkov radiation is generated when particles travel faster than light in a medium. For electrons in tissues, this energy threshold is about 0.219 MeV. It is proposed that a linear accelerator (LINAC), which is commonly used in RT in the clinic, can stimulate this phenomenon in body tissues. A clinic LINAC generates X-rays in the range of 6–18 MeV with about 80% photons and 20% electrons. It is reasoned that tissues under irradiation can serve as an in situ scintillator source, producing photons for PDT activation (Li, Mitchell, & Cherry, 2010). This approach is appealing because compared to radioisotopes, external beam induced Cherenkov radiation may provide a higher photon flux and thus more efficient PDT. A Monte Carlo simulation comparing the two found that the available photons for radioisotopes would be 0.01–1 nW/cm^2 and 1–100 μW/cm^2 for external RT beams, dependent on the given waveband, optical properties, and radiation source (Glaser et al., 2015).

External beam-based Cherenkov illumination has already been used to map tumor treatment during RT using a photosensitizer (Axelsson, Davis, Gladstone, & Pogue, 2011). With a water-based phantom, Axelsson et al. (2011) were able to activate the fluorophore PpIX (which has utility as a photosensitizer as well) and demonstrate that the higher the energy X-ray the greater the PpIX fluorescence, as follows via the Frank Tamm equation:

$$\frac{dN}{dx} = \frac{2\pi}{137}\left(\frac{1}{\lambda_1} - \frac{1}{\lambda_2}\right)\left(1 - \frac{1}{\beta^2 \eta_2}\right)$$

where η is refractive index and β is the Cherenkov threshold (Ross, 1969). The equation predicts that photon yield and path-length correlate to X-ray energy. The group was then able to demonstrate this phenomenon in vivo and in real time when they obtained video imaging breast cancer patients tumors with doses and energies comparable to those used in

RT (Jarvis et al., 2014). The group also hypothesized that if a photosensitizer were to be loaded into tumors, this CL could also be used for PDT. Based on the results of luminescence imaging studies discussed above, the group evaluated a theoretical approach for external beam CR-PDT. Taking a fractionation scheme representative of RT scheme: where 2 Gy is administered each day for 30 days, the daily light dose at 450 nm would be approximately 20 μJ/cm^2 and 32 μJ/cm^2 for 6 or 18 MV photon beam, respectively. The accumulated light dose, over 30 days, would be then 0.6 mJ/cm^2 and 1 mJ/cm^2 for the two photon beam energies. This would be lower flux than standard treatment, but significantly greater than that observed by radioisotopes PDT.

This technique is poised for potential synergies with explored techniques. As discussed above the presence of nanoscintillators have been shown to greatly enhance the CL generated by radionuclides. It is believed that an X-PDT nanoparticle agent developed to take advantage of the CL as well as the X-ray-induced scintillation would greatly enhance its tumor lethality. Another potential synergy between CL and nanoscintillators with optical down conversion. Cherenkov radiation mainly generates UV-blue wavelengths. This not only limits which photosensitizers are applicable but also has poor tissue penetration depth, reducing the quantity of usable photons. The use of a nanoparticle transducer to down-convert the energy could alleviate both of these issues. While to our knowledge none of these approaches have yet been explored it opens an interesting avenue for further enhancing X-PDT lethality as well as the synergistic effects between X-rays, PDT and nanoparticles.

5 | X-PDT AND CR-PDT: COMBINATION THERAPIES

X-PDT and CR-PDT were developed to address the tissue penetration problem of conventional PDT. But because the energy down-conversion is never 100%, and both approaches involve a significant RT component. In this sense, X-PDT and CR-PDT are in essence PDT and RT combinations, and the synergy between the two modalities might help explain the high treatment efficacy at a relatively low radiation doses.

The idea of combining PDT and RT was proposed decades ago (Ramakrishnan, Clay, Friedman, Antunez, & Oleinick, 1990). In most studies, PDT showed either an additive or synergistic effect when combined with RT. It seems that time interval between them is a critical factor. According to Kostron, Swartz, Miller, and Martuza (1986) when RT and PDT was applied sequentially with a 30-min gap, the therapy was additive, regardless of the treatment order. Within 30 minutes, however, synergistic benefits were observed. Others reported a much narrower interval for combination synergy. For instance, Kavarnos, Nath, and Bongiorni (1994) found that if given beyond 1 min apart the effect was not synergistic but additive. The mechanism was never fully understood but a popular postulation is that it derives from the fact that PDT and RT target different cellular organisms. Specifically, ionizing radiation mainly causes DNA strand breaks and RNA synthesis inhibition, resulting in cell apoptosis, mutation, and chromatic aberration (Luijsterburg & van Attikum, 2011). While the cellular impacts of PDT often involve damage to the lipids and plasma membrane, though these are photosensitizer-dependent (Dougherty et al., 1998). The combination may override cell repairs, leading to high lethality at a sublethal radiation dose (Luksiene, Kalvelyte, & Supino, 1999; Ramakrishnan et al., 1990).

Other mechanisms have been proposed to account for the synergy. Montazerabadi, Sazgarnia, Bahreyni-Toosi, Ahmadi, and Aledavood (2012) suggested that some PDT-resistant tumor cells are more sensitive to ionizing radiation and some radiation-resistant tumor cells are sensitive to PDT. Benstead and Moore (1990) proposed that rapid cancer cell death by PDT serves as selection pressure, causing cancer cells to replicate at an increased rate. This exacerbates the damage caused by radiation, which is most effective against fast proliferating cells. Rubin and Casarett (1968) hypothesized that late stage radiation damage is caused by the leakage of plasma into the interstitial space from a compromised epithelial lining. This stimulates fibrosis and leads to cell death. As PDT also leads to a leaky endothelial lining, when the two techniques are combined the probability of fibrosis is increased. These mechanisms seems less likely as the effect is observed only within a short time frame regardless if the RT occurs before after PDT. It should be noted that this synergistic effect has not universally been observed in all tumor models, and for a while not at all in clinical trials. However, some recent clinical studies have since shown an improvement in cure rate due to a synergistic effect between the RT and PDT (Kostron, Obwegeser, & Jakober, 1996; Nakano et al., 2011; Prinsze, Penning, Dubbelman, & VanSteveninck, 1992).

Despite the encouraging results, the PDT and RT combination has limited prospect in the clinic. This again is attributed to the shallow tissue penetration of light which limits the use of PDT. It is also challenging to colocalize the photo- and X-ray-irradiation to maximize synergy between the two modalities. The fact that a PDT session can take 15 min or longer while a RT session takes less than 5 min also poses difficulties for the combination. While the concept of PDT and RT combination is attractive, the interest has remained academic for most therapies.

The emergence of X-PDT and CR-PDT makes us revisit these early studies and find clues about the high treatment efficacy of these new modalities. In one recent study, we treated H1299 cells with SAO:Eu-mediated X-PDT and examined the impacts on cells through multiple assays (Wang et al., 2016). We found that X-PDT caused DNA damage and reduced clonogenicity, which are characteristics of RT. Meanwhile, X-PDT also induced early time point necrosis and increased lipid damage, suggesting a PDT component in the treatment. Western blotting and lipid peroxidation assay also found both RT and PDT patterns in X-PDT but suggested a shift of the impacts from DNA breaks in RT to lipid damage in PDT (Figure 3e). This evidence supports the notion that X-PDT is in essence RT and PDT combination. Unlike the conventional combination, however, in X-PDT and CR-PDT, one energy source simultaneously activates both processes. This makes the combination always in synchronism and the synergy potential maximized. The new approaches also overcome the tissue penetration problem, making the combination more clinically relevant and translation more feasible.

6 | CONCLUSION

Despite recent progress, X-PDT and CR-PDT development is still in its infancy. On one hand, encouraging results were observed at both in vitro and in vivo levels. On the other hand, no simulation models are able to fully explain the observed tumor therapy. In future

studies, it will be important to look into the energy transfer between scintillators and photosensitizers and determine the portion of radicals produced from the X-PDT mechanism. Crucially, X-PDT and CR-PDT are essentially RT and PDT combination therapy. How the two modalities interact and how they affect cells at DNA and molecular levels should be examined further.

One complication is the diversity in energy sources and scintillator nanoparticles. So far, the majority of X-PDT studies were conducted with low or medium energy X-ray beams. While at lower energies (20–170 keV) the photoelectric absorption component dominates Compton scattering by an order of magnitude as the energy increases, so does the Compton scattering component, reducing the enhancement seen by high Z elements in X-ray absorption (Takahashi & Misawa, 2007). It is important to test these nanoparticles with clinical MeV beams and see if the effectives can surpass the simulation studies. Another consideration is the toxicity from nanoparticles. Previous studies focus on scintillation materials with appealing optical properties but pay little attention on their bio-compatibility and bio-degradability. For future developments, the feasibility of clinical translation should become an important criterion.

Despite this, the future does look bright for X-PDT. Most of the current particles show increased tumor lethality over radiotherapy while exposing patients to lower X-ray doses. Additionally, there are vast numbers of scintillating nanoparticles, afterglow phosphors, medical isotopes that have yet to be adapted or optimized for X-PDT/CR-PDT. What can be achieved with external beam CR-PDT remains only theoretical at this point. It is believed that once the benefits are shown in vivo this area will quickly become one of the most exciting in X-PDT as it works in perfect conjunction with enhancing the effectiveness of classic X-PDT models. A further area of future exploration of PDT is in vasculature targeting. While PDT has demonstrated effective vasculature destruction, little analysis has been performed to see this effect in X-PDT. Given that many nanoparticles are too large for efficient extravasation, tumor vasculature is a promising target for future X-PDT. The principals behind X-PDT may have potential beyond the generation of ROSs. Y_2O_3 nanoparticles conjugated with psoralen (a photoactive drug) and after irradiation have formed monoaducts and cross-linking that induce apoptosis for deep tissue tumor treatment (Scaffidi, Gregas, Lauly, Zhang, & Vo-Dinh, 2011). Combining X-PDT nanosystems with other photoactive drugs instead of or in addition to photosensitizers is an unexplored territory with exciting opportunities.

ACKNOWLEDGMENTS

This work was supported by two National Institutes of Health grants (R01EB022596 and R01NS093314), one Congressionally Directed Medical Research Programs grant (CA140666), one National Science Foundation grant (NSF1552617).

Funding information

National Science Foundation, Grant/Award Number: NSF1552617; Congressionally Directed Medical Research Programs, Grant/Award Number: CA140666; National Institutes of Health, Grant/Award Numbers: R01NS093314, R01EB022596

REFERENCES

Agostinis P, Berg K, Cengel KA, Foster TH, Girotti AW, Gollnick SO, … Kessel D (2011). Photodynamic therapy of cancer: An update. CA: A Cancer Journal for Clinicians, 61(4), 250–281. [PubMed: 21617154]

Alivisatos AP (1996). Semiconductor clusters, nanocrystals, and quantum dots. Science, 271(5251), 933–937.

Axelsson J, Davis SC, Gladstone DJ, & Pogue BW (2011). Cerenkov emission induced by external beam radiation stimulates molecular fluorescence. Medical Physics, 38(7), 4127–132. [PubMed: 21859013]

Band I, Kharitonov YI, & Trzhaskovskaya M (1979). Photoionization cross sections and photoelectron angular distributions for X-ray line energies in the range 0.132–4.509 keV targets: 1≤ Z≤ 100. Atomic Data and Nuclear Data Tables, 23(5), 443–505.

Bellnier DA,& Lin C-W (1985). Photosensitization and split-dose recovery in cultured human urinary bladder carcinoma cells containing nonexchangeable hematoporphyrin derivative. Cancer Research, 45(6), 2507–2511. [PubMed: 3986790]

Benstead K, & Moore JV (1990). The effect of combined modality treatment with ionising radiation and TPPS-mediated photodynamic therapy on murine tail skin. British Journal of Cancer, 62(1), 48–53. [PubMed: 2390482]

Bistolfi F (2000). Red radioluminescence and radiochemiluminescence: Premises for a photodynamic tumour therapy with X-rays and haematoporphyrin derivatives. A working hypothesis. Panminerva Medica, 42(1), 69–75. [PubMed: 11019608]

Brus LE (1984). Electron–electron and electron-hole interactions in small semiconductor crystallites: The size dependence of the lowest excited electronic state. The Journal of Chemical Physics, 80(9), 4403–409.

Bulin A-L, Truillet C, Chouikrat R, Lux F, Frochot C, Amans D, … Barberi-Heyob M (2013). X-ray-induced singlet oxygen activation with nanoscintillator-coupled porphyrins. The Journal of Physical Chemistry C, 117(41), 21583–21589.

Bulin A-L, Vasil'Ev A, Belsky A, Amans D, Ledoux G, & Dujardin C (2015). Modelling energy deposition in nanoscintillators to predict the efficiency of the X-ray-induced photodynamic effect. Nanoscale, 7(13), 5744–5751. [PubMed: 25746211]

Cebim M, Oliveira H, Krauser M, & Davolos M (2017). X-ray-excited optical luminescence In Longo E & La Porta F (Eds.), Recent advances in complex functional materials (pp. 177–193). Cham, Switzerland: Springer.

Chen H, Sun X, Wang GD, Nagata K, Hao Z, Wang A, … Shen B (2017). LiGa 5 O 8: Cr-based theranostic nanoparticles for imaging-guided X-ray induced photodynamic therapy of deep-seated tumors. Materials Horizons, 4(6), 1092–1101.

Chen H, Wang F, Moore TL, Qi B, Sulejmanovic D, Hwu S-J, … Anker JN (2017). Bright X-ray and up-conversion nanophosphors annealed using encapsulated sintering agents for bioimaging applications. Journal of Materials Chemistry B, 5(27), 5412–5424. [PubMed: 29497532]

Chen H, Wang GD, Chuang Y-J, Zhen Z, Chen X, Biddinger P, … Pan Z (2015). Nanoscintillator-mediated X-ray inducible photodynamic therapy for in vivo cancer treatment. Nano Letters, 15(4), 2249–2256. [PubMed: 25756781]

Chen H, Wang GD, Tang W, Todd T, Zhen Z, Tsang C, … Xie J (2014). Gd-encapsulated carbonaceous dots with efficient renal clearance for magnetic resonance imaging. Advanced Materials, 26(39), 6761–6766. 10.1002/adma.201402964 [PubMed: 25178894]

Chen W, & Zhang J (2006). Using nanoparticles to enable simultaneous radiation and photodynamic therapies for cancer treatment. Journal of Nanoscience and Nanotechnology, 6(4), 1159–1166. [PubMed: 16736782]

Cherenkov P (1960). Radiation from high-speed particles. Science, 131(3394), 136–142. [PubMed: 13809644]

Ciarrocchi E, & Belcari N (2017). Cerenkov luminescence imaging: Physics principles and potential applications in biomedical sciences. EJNMMI Physics, 4(1), 14. [PubMed: 28283990]

Clement S, Chen W, Anwer AG, & Goldys EM (2017). Verteprofin conjugated to gold nanoparticles for fluorescent cellular bioimaging and X-ray mediated photodynamic therapy. Microchimica Acta, 184(6), 1765–1771.

Clement S, Deng W, Camilleri E, Wilson BC, & Goldys EM (2016). X-ray induced singlet oxygen generation by nanoparticle-photosensitizer conjugates for photodynamic therapy: Determination of singlet oxygen quantum yield. Scientific Reports, 6, 19954. [PubMed: 26818819]

Cooper DR, Bekah D, & Nadeau JL (2014). Gold nanoparticles and their alternatives for radiation therapy enhancement. Frontiers in Chemistry, 2, 86. [PubMed: 25353018]

Cooper DR, Capobianco JA, & Seuntjens J (2018). Radioluminescence studies of colloidal oleate-capped β-Na (Gd, Lu) F 4: Ln 3+ nanoparticles (Ln= Ce, Eu, Tb). Nanoscale, 10, 7821–7832. [PubMed: 29664089]

Davis ME, & Shin DM (2008). Nanoparticle therapeutics: An emerging treatment modality for cancer. Nature Reviews Drug Discovery, 7(9), 771–782. [PubMed: 18758474]

Dougherty TJ, Gomer CJ, Henderson BW, Jori G, Kessel D, Korbelik M, … Peng Q (1998). Photodynamic therapy. Journal of the National Cancer Institute, 90(12), 889–905. [PubMed: 9637138]

Dujardin C, Amans D, Belsky A, Chaput F, Ledoux G, & Pillonnet A (2010). Luminescence and scintillation properties at the nanoscale. IEEE Transactions on Nuclear Science, 57(3), 1348–1354.

Elmenoufy AH, Tang Y. a., Hu J, Xu H, & Yang X (2015). A novel deep photodynamic therapy modality combined with CT imaging established via X-ray stimulated silica-modified lanthanide scintillating nanoparticles. Chemical Communications, 51(61), 12247–12250. [PubMed: 26136105]

Emberton M (2016). TOOKAD (Padeliporfin) vascular-targeted photodynamic therapy versus active surveillance in men with low risk prostate cancer. A randomized phase 3 clinical trial. Abstract LBA02. Copenhagen, Denmark: European Association of Urology (EAU) Congress.

Fabbri F, Rossi F, Attolini G, Salviati G, Dierre B, Sekiguchi T, & Fukata N (2012). Luminescence properties of SiC/SiO 2 core–shell nanowires with different radial structure. Materials Letters, 71, 137–140.

Fei Q, Chang C, & Mao D (2005). Luminescent properties of Sr 2 MgSi 2 O 7 and ca 2 MgSi 2 O 7 long lasting phosphors activated by Eu 2+, Dy 3+. Journal of Alloys and Compounds, 390(1), 133–137.

Gaspar R, Mazali I, & Sigoli F (2010). Particle size tailoring and luminescence of europium (III)-doped gadolinium oxide obtained by the modified homogeneous precipitation method: Dielectric constant and counter anion effects. Colloids and Surfaces A: Physicochemical and Engineering Aspects, 367(1−3), 155–160.

Generalov R, Kuan WB, Chen W, Kristensen S, & Juzenas P (2015). Radiosensitizing effect of zinc oxide and silica nanocomposites on cancer cells. Colloids and Surfaces B: Biointerfaces, 129, 79–86. [PubMed: 25829130]

Glaser AK, Zhang R, Andreozzi JM, Gladstone DJ, & Pogue BW (2015). Cherenkov radiation fluence estimates in tissue for molecular imaging and therapy applications. Physics in Medicine & Biology, 60(17), 6701–6718. [PubMed: 26270125]

Gollnick SO, Vaughan L, & Henderson BW (2002). Generation of effective antitumor vaccines using photodynamic therapy. Cancer Research, 62(6), 1604–1608. [PubMed: 11912128]

Gonzales J, Wang F, Zamora G, Trinidad A, Marcu L, Cherry S, & Hirschberg H (2014). Ultra low fluence rate photodynamic therapy: Simulation of light emitted by the Cerenkov effect. Paper presented at Proceedings of SPIE 8928, Optical Techniques in Neurosurgery, Neurophotonics, and Optogenetics, 89280F, San Francisco, CA, USA.

Hamieh M, Dorkenoo K, Taupier G, Henry Y, & Halley D (2017). Evidence of a permanent electric polarisation in highly strained Cr2O3 clusters measured by a second harmonic generation technique. Journal of Physics: Condensed Matter, 29(20), 205301. [PubMed: 28338475]

Hartl BA, Hirschberg H, Marcu L, & Cherry SR (2016). Activating photodynamic therapy in vitro with cerenkov radiation generated from yttrium-90. Journal of Environmental Pathology, Toxicology and Oncology, 35(2), 185–192.

Henderson BW, Busch TM, & Snyder JW (2006). Fluence rate as a modulator of PDT mechanisms. Lasers in Surgery and Medicine, 38(5), 489–493. [PubMed: 16615136]

Homayoni H, Ma L, Zhang J, Sahi SK, Rashidi LH, Bui B, & Chen W (2016). Synthesis and conjugation of Sr2MgSi2O7: Eu2+, Dy3+ water soluble afterglow nanoparticles for photodynamic activation. Photodiagnosis and Photodynamic Therapy, 16, 90–99. [PubMed: 27594671]

Hoogendam JP, Zweemer RP, Hobbelink MG, Van Den Bosch MA, Verheijen RH, & Veldhuis WB (2016). 99mTC-Nanocolloid SPECT/MRI fusion for the selective assessment of nonenlarged sentinel lymph nodes in patients with early-stage cervical cancer. Journal of Nuclear Medicine, 57(4), 551–556. [PubMed: 26678614]

Hopper C (2000). Photodynamic therapy: A clinical reality in the treatment of cancer. The Lancet Oncology, 1(4), 212–219. [PubMed: 11905638]

Hsu C-C, Lin S-L, & Chang CA (2018). Lanthanide-doped core–shell–shell nanocomposite for dual photodynamic therapy and luminescence imaging by a single X-ray excitation source. ACS Applied Materials & Interfaces, 10(9), 7859–7870. [PubMed: 29405703]

Huang Z (2005). A review of progress in clinical photodynamic therapy. Technology in Cancer Research & Treatment, 4(3), 283–293. [PubMed: 15896084]

Huang Z, Xu H, Meyers AD, Musani AI, Wang L, Tagg R, … Chen YK (2008). Photodynamic therapy for treatment of solid tumors—Potential and technical challenges. Technology in Cancer Research & Treatment, 7(4), 309–320. [PubMed: 18642969]

Jarvis LA, Zhang R, Gladstone DJ, Jiang S, Hitchcock W, Friedman OD, … Pogue BW (2014). Cherenkov video imaging allows for the first visualization of radiation therapy in real time. International Journal of Radiation Oncology, Biology, Physics, 89(3), 615–622.

Jung J, Hirata G, Gundiah G, Derenzo S, Wrasidlo W, Kesari S, … McKittrick J (2014). Identification and development of nanoscintillators for biotechnology applications. Journal of Luminescence, 154, 569–577.

Justel T, & Feldmann C (2007). Radiation therapy and medical imaging using UV emitting nanoparticles. USA: IFI CLAIMS Patent Services.

Kalka K, Merk H, & Mukhtar H (2000). Photodynamic therapy in dermatology. Journal of the American Academy of Dermatology, 42(3), 389–413. [PubMed: 10688709]

Kamkaew A, Cheng L, Goel S, Valdovinos HF, Barnhart TE, Liu Z, & Cai W (2016). Cerenkov radiation induced photodynamic therapy using Chlorin e6-loaded hollow mesoporous silica nanoparticles. ACS Applied Materials & Interfaces, 8(40), 26630–26637. [PubMed: 27657487]

Kaščáková S, Giuliani A, Lacerda S, Pallier A, Mercère P, Tóth É, & Réfrégiers M (2015). X-ray-induced radiophotodynamic therapy (RPDT) using lanthanide micelles: Beyond depth limitations. Nano Research, 8(7), 2373–2379.

Kavarnos G, Nath R, & Bongiorni P (1994). Visible-light and X irradiations of Chinese hamster lung cells treated with hematoporphyrin derivative. Radiation Research, 137(2), 196–201. [PubMed: 8134543]

Kelloff GJ, Hoffman JM, Johnson B, Scher HI, Siegel BA, Cheng EY, … Mankoff DA (2005). Progress and promise of FDG-PET imaging for cancer patient management and oncologic drug development. Clinical Cancer Research, 11(8), 2785–2808. [PubMed: 15837727]

Kim H-T, Kim K-H, Choi G-H, Jheon S, Park S-H, Kim B-I, … Kim J-K (2009). Photodynamic synchrotron x-ray therapy in Glioma cell using superpara-magnetic iron nanoparticle. Paper presented at Proceedings of Photodynamic Therapy: Back to the Future, Seattle, WA, USA.

Kirakci K, Kubát P, Fejfarová K, Martinčík J. í., Nikl M, & Lang K (2015). X-ray inducible luminescence and singlet oxygen sensitization by an octahedral molybdenum cluster compound: A new class of Nanoscintillators. Inorganic Chemistry, 55(2), 803–809. [PubMed: 26702498]

Klassen N, Smyt'ko I, Strukova G, Kedrov V, Kobelev N, Kudrenko E, … Prokopiuk N (2005). Improvement of scintillation parameters in complex oxides by formation of nanocrystalline structures. Paper presented at Proceedings of 8th International SCINT Conference, Crimea, Ukraine.

Korbelik M (2011). Cancer vaccines generated by photodynamic therapy. Photochemical & Photobiological Sciences, 10(5), 664–669. [PubMed: 21258728]

Kostron H, Obwegeser A, & Jakober R (1996). Photodynamic therapy in neurosurgery: A review. Journal of Photochemistry and Photobiology B: Biology, 36(2), 157–168.

Kostron H, Swartz MR, Miller DC, & Martuza RL (1986). The interaction of hematoporphyrin derivative, light, and ionizing radiation in a rat glioma model. Cancer, 57(5), 964–970. [PubMed: 3943032]

Kotagiri N, Cooper ML, Rettig M, Egbulefu C, Prior J, Cui G, … Sudlow G (2018). Radionuclides transform chemotherapeutics into phototherapeutics for precise treatment of disseminated cancer. Nature Communications, 9(1), 275.

Kotagiri N, Sudlow GP, Akers WJ, & Achilefu S (2015). Breaking the depth dependency of phototherapy with Cerenkov radiation and low-radiance-responsive nanophotosensitizers. Nature Nanotechnology, 10(4), 370–379.

Lan G, Ni K, Xu R, Lu K, Lin Z, Chan C, & Lin W (2017). Nanoscale metal–organic layers for deeply penetrating X-ray-induced photodynamic therapy. Angewandte Chemie, 129(40), 12270–12274.

Ledoux G, Gong J, Huisken F, Guillois O, & Reynaud C (2002). Photoluminescence of size-separated silicon nanocrystals: Confirmation of quantum confinement. Applied Physics Letters, 80(25), 4834–4836.

Ledoux G, Mercier B, Louis C, Dujardin C, Tillement O, & Perriat P (2004). Synthesis and optical characterization of Gd2O3: Eu3+ nanocrystals: Surface states and VUV excitation. Radiation Measurements, 38(4–6), 763–766.

Lempicki A, Wojtowicz A, & Berman E (1993). Fundamental limits of scintillator performance. Nuclear Instruments and Methods in Physics Research Section A: Accelerators, Spectrometers, Detectors and Associated Equipment, 333(2–3), 304–311.

Li C, Mitchell GS, & Cherry SR (2010). Cerenkov luminescence tomography for small-animal imaging. Optics Letters, 35(7), 1109–1111. [PubMed: 20364233]

Li N, Yu L, Wang J, Gao X, Chen Y, Pan W, & Tang B (2018). A mitochondria-targeted nanoradiosensitizer activating reactive oxygen species burst for enhanced radiation therapy. Chemical Science, 9(12), 3159–3164. [PubMed: 29732098]

Li S, Liu Y, Liu C, Yan D, Zhu H, Yang J, … Wang X (2017). Design, fabrication and characterization of nanocaged 12CaO· 7Al2O3: Tb3+ photostimulable phosphor for high-quality X-ray imaging. Materials & Design, 134, 1–9.

Liu J, Yang Y, Zhu W, Yi X, Dong Z, Xu X, … Jiang L (2016). Nanoscale metal– organic frameworks for combined photodynamic & radiation therapy in cancer treatment. Biomaterials, 97, 1–9. [PubMed: 27155362]

Liu X, Chen Y, Li H, Huang N, Jin Q, Ren K, & Ji J (2013). Enhanced retention and cellular uptake of nanoparticles in tumors by controlling their aggregation behavior. ACS Nano, 7(7), 6244–6257. [PubMed: 23799860]

Losytskyy MY, Kuzmenko LV, Shcherbakov OB, Gamaleia NF, Marynin AI, & Yashchuk VM (2017). Energy transfer in Ce 0.85 Tb 0.15 F 3 nanoparticles-CTAB Shell-Chlorin e 6 system. Nanoscale Research Letters, 12(1), 294. [PubMed: 28445996]

Losytskyy MY, Vretik L, Nikolaeva O, Marynin A, Gamaleya N, & Yashchuk V (2016). Polystyrene-diphenyloxazole-chlorin e6 nanosystem for PDT: Energy transfer study. Molecular Crystals and Liquid Crystals, 639(1), 169–176.

Lu K, He C, & Lin W (2015). A chlorin-based nanoscale metal-organic framework for photodynamic therapy of colon cancers. Journal of the American Chemical Society, 137(24), 7600–7603. [PubMed: 26068094]

Luijsterburg MS, & van Attikum H (2011). Chromatin and the DNA damage response: The cancer connection. Molecular Oncology, 5(4), 349–367. [PubMed: 21782533]

Luksiene Z, Kalvelyte A, & Supino R (1999). On the combination of photodynamic therapy with ionizing radiation. Journal of Photochemistry and Photobiology B: Biology, 52(1–3), 35–2.

Ma L, Zou X, Bui B, Chen W, Song KH, & Solberg T (2014). X-ray excited ZnS: Cu, co afterglow nanoparticles for photodynamic activation. Applied Physics Letters, 105(1), 013702.

Ma L, Zou X, & Chen W (2014). A new X-ray activated nanoparticle photosensitizer for cancer treatment. Journal of Biomedical Nanotechnology, 10(8), 1501–1508. [PubMed: 25016650]

Maisch T, Baier J, Franz B, Maier M, Landthaler M, Szeimies R-M, & Bäumler W (2007). The role of singlet oxygen and oxygen concentration in photodynamic inactivation of bacteria. Proceedings of the National Academy of Sciences, 104(17), 7223–7228.

Majumder D, Choudhury K, Das P, Kundu S, & Mitra D (2013). Different fractionation schedules of radiotherapy in locally advanced head and neck malignancy: A prospective randomized study to compare the results of treatment and toxicities of different protocols. South Asian Journal of Cancer, 2(1), 31–35. [PubMed: 24455542]

Marchetti B, & Karsili TN (2016). An exploration of the reactivity of singlet oxygen with biomolecular constituents. Chemical Communications, 52(73), 10996–10999. [PubMed: 27538187]

Montazerabadi AR, Sazgarnia A, Bahreyni-Toosi MH, Ahmadi A, & Aledavood A (2012). The effects of combined treatment with ionizing radiation and indocyanine green-mediated photodynamic therapy on breast cancer cells. Journal of Photochemistry and Photobiology B: Biology, 109, 42–49.

Morgan NY, Kramer-Marek G, Smith PD, Camphausen K, & Capala J (2009). Nanoscintillator conjugates as photodynamic therapy-based radiosensitizers: Calculation of required physical parameters. Radiation Research, 171(2), 236–244. [PubMed: 19267550]

Muenchausen RE, McKigney EA, Jacobsohn LG, Blair MW, Bennett BL, & Cooke DW (2008). Science and application of oxyorthosilicate nanophosphors. IEEE Transactions on Nuclear Science, 55(3), 1532–1535.

Nakano A, Watanabe D, Akita Y, Kawamura T, Tamada Y, & Matsumoto Y (2011). Treatment efficiency of combining photodynamic therapy and ionizing radiation for Bowen's disease. Journal of the European Academy of Dermatology and Venereology, 25(4), 475–478. [PubMed: 20569287]

Nanda K, Kruis F, Fissan H, & Behera S (2004). Effective mass approximation for two extreme semiconductors: Band gap of PbS and CuBr nanoparticles. Journal of Applied Physics, 95(9), 5035–5041.

Niedre MJ, Secord AJ, Patterson MS, & Wilson BC (2003). In vitro tests of the validity of singlet oxygen luminescence measurements as a dose metric in photodynamic therapy. Cancer Research, 63(22), 7986–7994. [PubMed: 14633731]

Noone AM, Howlader N, Krapcho M, Miller D, Brest A, Yu M, … Cronin KA (Eds.). (2018). SEER cancer statistics review, 1975–2015. Bethesda, MD: National Cancer Institute Retrieved from https://seer.cancer.gov/csr/1975_2015/

Oseroff A (2006). PDT as a cytotoxic agent and biological response modifier: Implications for cancer prevention and treatment in immunosuppressed and immunocompetent patients. Journal of Investigative Dermatology, 126(3), 542–544. [PubMed: 16482195]

Packer S (1984). Tumor detection with radiopharmaceuticals. Seminars in Nuclear Medicine, 14(1), 21–30. [PubMed: 6369546]

Paillard V, Puech P, Laguna M, Carles R, Kohn B, & Huisken F (1999). Improved one-phonon confinement model for an accurate size determination of silicon nanocrystals. Journal of Applied Physics, 86(4), 1921–1924.

Park J, Jiang Q, Feng D, Mao L, & Zhou H-C (2016). Size-controlled synthesis of porphyrinic metal–organic framework and functionalization for targeted photodynamic therapy. Journal of the American Chemical Society, 138(10), 3518–3525. [PubMed: 26894555]

Pereira A, Martin T, Levinta M, & Dujardin C (2015). Low-absorption, multi-layered scintillating material for high resolution real-time X-ray beam analysis. Journal of Materials Chemistry C, 3(19), 4954–4959.

Phillips E, Penate-Medina O, Zanzonico PB, Carvajal RD, Mohan P, Ye Y, … Schöder H (2014). Clinical translation of an ultrasmall inorganic optical-PET imaging nanoparticle probe. Science Translational Medicine, 6(260), 260ra149.

Pratt EC, Shaffer TM, & Grimm J (2016). Nanoparticles and radiotracers: Advances toward radionanomedicine. WIREs Nanomedicine and Nanobiotechnology, 8(6), 872–890. [PubMed: 27006133]

Pratt EC, Shaffer TM, Zhang Q, Drain CM, & Grimm J (2018). Nanoparticles as multimodal photon transducers of ionizing radiation. Nature Nanotechnology, 13(1), 418–26.

Pratx G, & Kapp DS (2018). Is Cherenkov luminescence bright enough for photodynamic therapy? Nature Nanotechnology, 13(5), 354–354. 10.1038/s41565-018-0142-y

Prinsze C, Penning LC, Dubbelman TM, & VanSteveninck J (1992). Interaction of photodynamic treatment and either hyperthermia or ionizing radiation and of ionizing radiation and hyperthermia with respect to cell killing of L929 fibroblasts, Chinese hamster ovary cells, and T24 human bladder carcinoma cells. Cancer Research, 52(1), 117–120. [PubMed: 1727371]

Rama Krishna MV, & Friesner R (1991). Quantum confinement effects in semiconductor clusters. The Journal of Chemical Physics, 95(11), 8309–8322.

Ramakrishnan N, Clay ME, Friedman LR, Antunez AR, & Oleinick NL (1990). Post-treatment interactions of photodynamic and radiation-induced cytotoxic lesions. Photochemistry and Photobiology, 52(3), 555–559. [PubMed: 2284348]

Robertson R, Germanos MS, Li C, Mitchell GS, Cherry SR, & Silva MD (2009). Optical imaging of Cerenkov light generation from positron-emitting radiotracers. Physics in Medicine and Biology, 54(16), N355–N365. [PubMed: 19636082]

Ross HH (1969). Measurement of beta-emitting nuclides using Cerenkov radiation. Analytical Chemistry, 41(10), 1260–1265.

Rossi F, Bedogni E, Bigi F, Rimoldi T, Cristofolini L, Pinelli S, … Attolini G (2015). Porphyrin conjugated SiC/SiOx nanowires for X-ray-excited photodynamic therapy. Scientific Reports, 5, 7606. [PubMed: 25556299]

Rubin PC, & Casarett GW (1968). Clinical radiation pathology as applied to curative radiotherapy. Cancer, 22(4), 767–778. [PubMed: 5212301]

Scaffidi JP, Gregas MK, Lauly B, Zhang Y, & Vo-Dinh T (2011). Activity of psoralen-functionalized nanoscintillators against cancer cells upon X-ray excitation. ACS Nano, 5(6), 4679–4687. [PubMed: 21553850]

Sengar P, Juárez P, Verdugo-Meza A, Arellano DL, Jain A, Chauhan K, … Fournier PG (2018). Development of a functionalized UV-emitting nanocomposite for the treatment of cancer using indirect photodynamic therapy. Journal of Nanobiotechnology, 16(1), 19. [PubMed: 29482561]

Shaffer TM, Pratt EC, & Grimm J (2017). Utilizing the power of Cerenkov light with nanotechnology. Nature Nanotechnology, 12(2), 106–117.

Sheng K, Li J, Weiss S, & Wang L (2012). MO-A-213AB-05: Synthesis of high quantum yield nano-scintillators for simultaneous photodynamic therapy in radiotherapy. Medical Physics, 39(6), 3859–3860.

Song L, Li PP, Yang W, Lin XH, Liang H, Chen XF, … Yang HH (2018). Low-dose X-ray activation of W (VI)-doped persistent luminescence nanoparticles for deep-tissue photodynamic therapy. Advanced Functional Materials, 28, 1707496.

Sudheendra L, Das GK, Li C, Stark D, Cena J, Cherry S, & Kennedy IM (2014). Nagdf4: Eu3+ nanoparticles for enhanced x-ray excited optical imaging. Chemistry of Materials, 26(5), 1881–1888. [PubMed: 24803724]

Takahashi J, & Misawa M (2007). Analysis of potential radiosensitizing materials for X-ray-induced photodynamic therapy. NanoBiotechnology, 3(2), 116–126. 10.1007/s12030-008-9009-x

Tang Y. a., Hu J, Elmenoufy AH, & Yang X (2015). Highly efficient FRET system capable of deep photodynamic therapy established on x-ray excited mesoporous LaF3: Tb scintillating nanoparticles. ACS Applied Materials & Interfaces, 7(22), 12261–12269. [PubMed: 25974980]

Thorek DL, Ogirala A, Beattie BJ, & Grimm J (2013). Quantitative imaging of disease signatures through radioactive decay signal conversion. Nature Medicine, 19(10), 1345–1350.

Townley HE, Kim J, & Dobson PJ (2012). In vivo demonstration of enhanced radiotherapy using rare earth doped titania nanoparticles. Nanoscale, 4(16), 5043–5050. [PubMed: 22767269]

Urruticoechea A, Alemany R, Balart J, Villanueva A, Vinals F, & Capella G (2010). Recent advances in cancer therapy: An overview. Current Pharmaceutical Design, 16(1), 3–10. [PubMed: 20214614]

van Duijnhoven FH, Aalbers RI, Rovers JP, Terpstra OT, & Kuppen PJ (2003). The immunological consequences of photodynamic treatment of cancer, a literature review. Immunobiology, 207(2), 105–113. [PubMed: 12675268]

Vistovskyy V, Malyi T, Vas'kiv A, Chylii M, Mitina N, Zaichenko A, … Voloshinovskii A (2016). Luminescent properties of LuPO4-Pr and LuPO4-Eu nanoparticles. Journal of Luminescence, 179, 527–532.

Vistovskyy V, Zhyshkovych A, Halyatkin O, Mitina N, Zaichenko A, Rodnyi P, … Voloshinovskii A (2014). The luminescence of BaF2 nanoparticles upon high-energy excitation. Journal of Applied Physics, 116(5), 054308.

Viswanatha R, Sapra S, Satpati B, Satyam P, Dev B, & Sarma D (2004). Understanding the quantum size effects in ZnO nanocrystals. Journal of Materials Chemistry, 14(4), 661–668.

Wahid K, Pokhrel M, & Mao Y (2017). Structural, photoluminescence and radioluminescence properties of Eu 3+ doped La 2 Hf 2 O 7 nanoparticles. Journal of Solid State Chemistry, 245, 89–97.

Wang C, Volotskova O, Lu K, Ahmad M, Sun C, Xing L, & Lin W (2014). Synergistic assembly of heavy metal clusters and luminescent organic bridging ligands in metal–organic frameworks for highly efficient X-ray scintillation. Journal of the American Chemical Society, 136(17), 6171–6174. [PubMed: 24730683]

Wang GD, Nguyen HT, Chen H, Cox PB, Wang L, Nagata K, … Xie J (2016). X-ray induced photodynamic therapy: A combination of radiotherapy and photodynamic therapy. Theranostics, 6(13), 2295–2305. [PubMed: 27877235]

Williams LE, DeNardo GL, & Meredith RF (2008). Targeted radionuclide therapy. Medical Physics, 35(7Part1), 3062–3068. [PubMed: 18697529]

Yang W, Read PW, Mi J, Baisden JM, Reardon KA, Larner JM, … Sheng K (2008). Semiconductor nanoparticles as energy mediators for photosensitizer-enhanced radiotherapy. International Journal of Radiation Oncology, Biology, Physics, 72(3), 633–635.

Yefimova S, Tkacheva T, Maksimchuk P, Bespalova I, Hubenko K, Klochkov V, … Malyukin YV (2017). GdVO4: Eu3+ nanoparticles–methylene blue complexes for PDT: Electronic excitation energy transfer study. Journal of Luminescence, 192, 975–981.

Yuan X, Setyawati MI, Tan AS, Ong CN, Leong DT, & Xie J (2013). Highly luminescent silver nanoclusters with tunable emissions: Cyclic reduction-decomposition synthesis and antimicrobial properties. NPG Asia Materials, 5(2), e39.

Zhang C, Zhao K, Bu W, Ni D, Liu Y, Feng J, & Shi J (2015). Marriage of scintillator and semiconductor for synchronous radiotherapy and deep photodynamic therapy with diminished oxygen dependence. Angewandte Chemie International Edition, 54(6), 1770–1774. [PubMed: 25483028]

Zou X, Yao M, Ma L, Hossu M, Han X, Juzenas P, & Chen W (2014). X-ray-induced nanoparticle-based photodynamic therapy of cancer. Nanomedicine, 9(15), 2339–2351. [PubMed: 24471504]

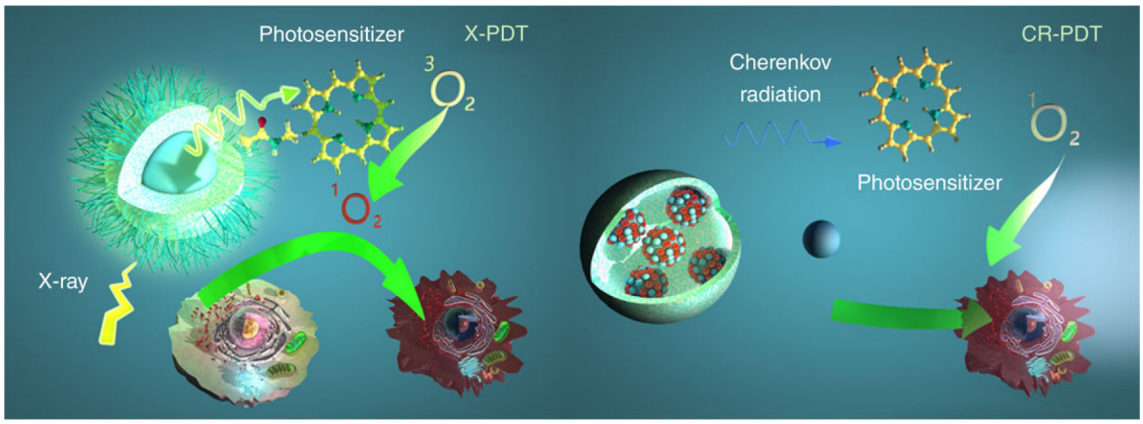

FIGURE 1.

Schematic illustration for X-PDT and CR-PDT. Left: Classic X-PDT. X-rays excite a nanoscintillator to generate X-ray luminescence, which in turn activate a photosensitizer to produce cytotoxic ROS. Right: Cherenkov radiation PDT. Cherenkov radiation from radioisotopes is harnessed to activate a photosensitizer to initiate PDT

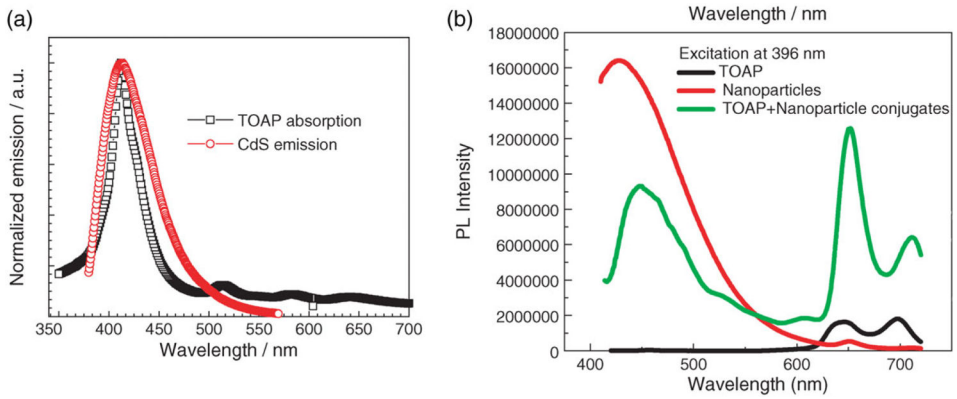

FIGURE 2.

(a) The emission spectrum (red) of CdS nanoparticles and the absorption spectrum (black) of tretrakis (*o*-aminophenyl) porphyrin (TOAP). (b) Fluorescence emission spectra of TOAP (black), CdS nanoparticles (green), and TOAP-CdS nanoparticle conjugates (red) (Reprinted with permission from W. Chen and Zhang (2006). Copyright 2006 American Scientific Publishers)

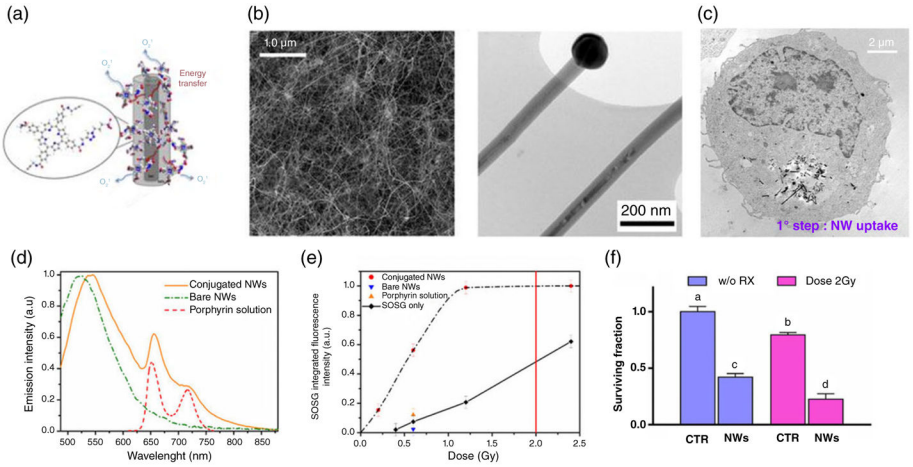

FIGURE 3.

Silica nanowire based X-PDT. (a) Schematic of the SiC/SiOx/H_2TPACPP system. Grown nanowires are functionalized with azide groups; the H_2TCPP porphyrin derivative containing an alkyne group (H2TPACPP) is synthesized by converting the carboxy groups into N-propynylamides; the nanohybrid is constructed by bonding H_2TPACPP to the NWs. (b) Left: SEM image of the as-grown nanowire network on Si substrate. Right: TEM image of two neighbor nanowires. (c) TEM of cellular uptake and internalization of the nanowires during the first 24 hr. (d) Fluorescence spectra acquired at room temperature over as-grown nanowires. (e) $^1O_2$ generated, as a function of the radiation dose. (f) Histogram of clongenic survival assay. (Reprinted with permission from Rossi et al. (2015). Copyright 2015 Nature Publishing Group)

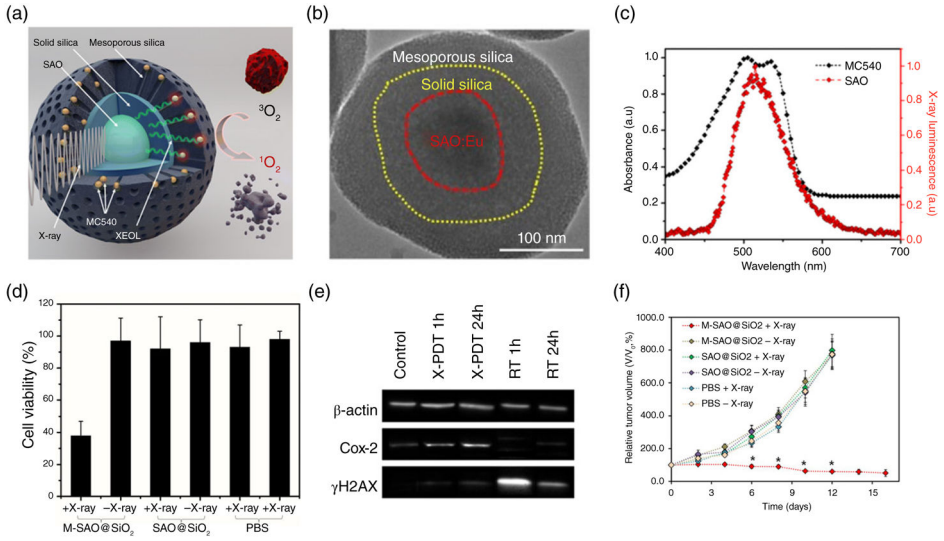

FIGURE 4.

X-PDT with strontium aluminum oxide (SAO) nanoparticles. (a) Schematic illustration of the working mechanism. A SAO nanoparticle core is coated with two layers of silica. MC540, a photosensitizer of matching, is loaded into the mesoporous layer. (b) TEM image of SAO@SiO_2 nanoparticles. (c) Comparison between the XEOL of SAO (red) and the absorbance of MC540 (black). (d) MTT assays showing that SAO nanoparticle-mediated X-PDT efficiently killed U87MG cells. (e) Western blotting assays. In the presence of SAO nanoparticles, radiation-induced cellular damage is shifted from DNA breaks to lipid peroxidation. (f) in vivo X-PDT therapy results. (Reprinted with permission from Hongmin Chen et al., (2015) and G. D. Wang et al., (2016). Copyright 2015 and 2016 American Chemical Society)

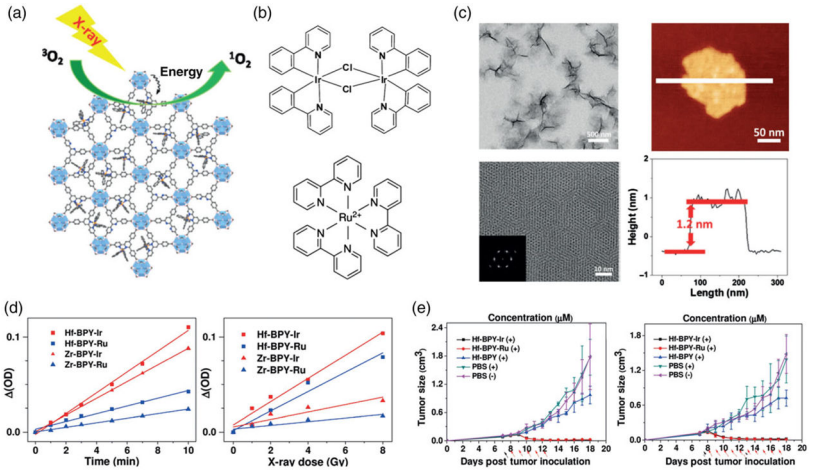

FIGURE 5.

Nanoscale metal organic layers for X-PDT. (a) Schematic for Hf-based nMOL X-PDT agent. (b) Photosensitizers. Top: Ir[2,2′-bipyridine (2-phenylpyridine)$_2$]$^+$. Bottom: [Ru(2,2′-bipyridine)$_3$]^{2}+ **c**) physical characterization. Top left: TEM nMOL bottom left: HRTEM image, inset: FFT pattern. Top right: Tapping-mode AFM topography. Bottom right: Height profile along the white line. **d**) SOSG assay results. Samples were treated by 225 kVp irradiation. (e) in vivo therapeutic effect of nMOL (left:CT26, right:MC38). (Reprinted with permission from Lan et al. (2017). Copyright 2017 John Wiley and Sons)

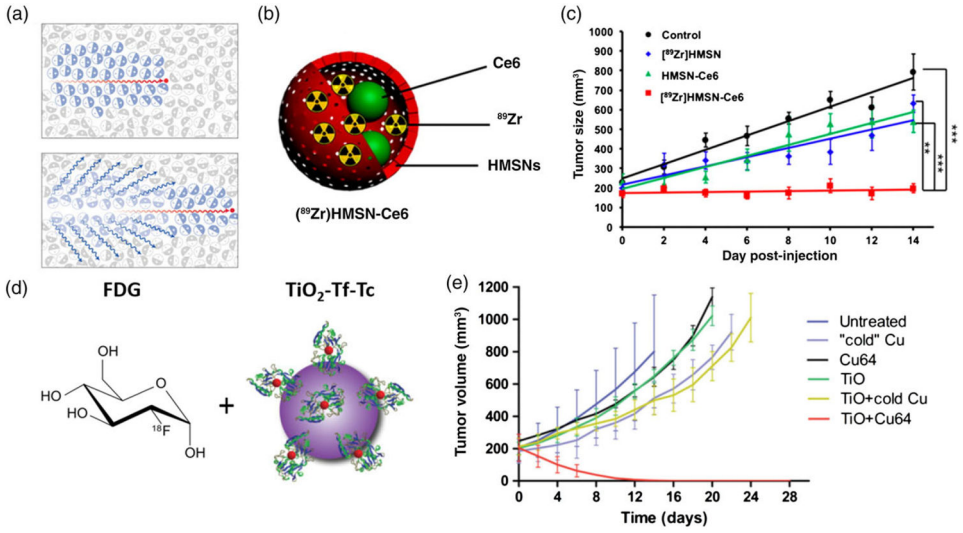

FIGURE 6.

(a) Schematic for Cherenkov radiation. (b) Chenekov X-PDT particle [^{89}Zr]HMSN-Ce6 schematic, (c) in vivo therapy results with [^{89}Zr]HMSN-Ce6. (d) Cherenkov X-PDT with a co-localization approach using 2-deoxy-2′-(^{18}F)fluoro-D-glucose and TiO_2-Tf-Tc nanoparticles. (e) Co-localization in vivo therapy results. (Reprinted with permission from Shaffer et al. (2017), Kamkaew et al. (2016) and Kotagiri et al. (2018). Copyright 2017, 2016 and 2018 American Chemical Society and Nature Publishing Group)

TABLE 1

X-PDT agents made by coupling a nanoscintillator and a photosensitizer

References	X-ray scintillator (emission)	Photosensitizer (absorption)	Particle size	X-ray energetics	Results
Chen and Zhang (2006)	CdS(420 nm)	Tretrakis (o-aminophenyl) porphyrin (400 nm)	—	—	Spectra
Clement et al. (2016)	CeF_3(340 nm)	Verteporfin (370,420 nm)	9nm	6 MeV, 30 keV 1–6 Gy	Singlet oxygen in vitro
Chen et al. (2015)	$SrAl_2O_4:Eu^{2+}$(520 nm), Silica coated	Merocyanine 540 (540 nm)	407 nm	50 keV 1–10 Gy	Singlet oxygen in vitro in vivo
Zou et al. (2014)	$LaF_3:Ce^{3+}$ (520 nm) PLGA encapsulated	Protoporphyrin IX (409 nm)	2 μm	90 keV, 3 Gy	Singlet oxygen in vitro
Tang et al. (2015)	LaF_3:Tb (544 nm)	Rose Bengal (560 nm)	40 nm	75 keV	Singlet oxygen
Elmenoufy et al. (2015)	LaF_3:Tb silica coated (540 nm)	Rose Bengal (560 nm)	45 nm	75 keV	Singlet Cxygen CT imaging
(Fabbri et al., 2012)	SiC/SiO_x core/shell nanowires (545 nm)	Tetracarboxyphenyl porphyrin derivative (550 nm)	Diameter 40 nm	6 MeV, 0.4–2 Gy	Singlet oxygen in vitro
Chen, Wang, et al. (2017)	LaF_3:Tb (540 nm)	Meso-tetra(4-carboxyphenyl)porphyrin (516 nm)	25 nm	80 keV	In vitro
Bulin et al. (2013)	Tb_2O_3 coated with polysiloxane (540 nm)	5-(4-carboxyphenyl)-10,15,20-triphenyl porphyrin (520 nm)	10 nm	44 keV, 11 Gy	Singlet oxygen
Kaščáková et al. (2015))	GdEuC12 (595 nm)	Hypericin (590 nm)	4.6	15 keV	Singlet oxygen cellular uptake
Lan et al. (2017)	HfnMOL (500 nm)	$Ir[2,2'\text{-bipyridine}(2\text{-phenylpyridine})_2]^+$(355 nm) Or $[Ru(2,2'\text{-bipyridine})_3]^{2+}$ (450 nm)	1.2 nmthickness	225 keV, 2 Gy	Singlet oxygen in vitro in vivo
Ma, Zou, and Chen (2014)	ZnS:Cu,co (510 nm)	TBrRh123 (518 nm)	4 nm	120 keV, 2 Gy	In vitro
Zhang et al. (2015)	$LiYF_4$:Ce (305 nm)	ZnO (290 nm)	35 nm	220 keV, 8 Gy	ROS production in vitro in vivo
Chen, Sun, et al. (2017)	$LiGa_5O_8$:Cr (720 nm)	2,3-naphthalocyanine (775 nm)	100 nm	50 keV, 5 Gy	Singlet oxygen
Hsu et al. (2018)	$NaLuF_4$:Gd,Eu @$NaLuF_4$:Gd @$NaLuF_4$:GdTb (543 nm)	Rose Bengal (560 nm)	25 nm	160 keV, 5 Gy	Singlet oxygen in vitro
Clement, Chen, Anwer, and Goldys (2017)	Au (not determined)	Verteprofin (365, 690 nm)	12 nm	6 MeV, 6 Gy	Singlet oxygen in vitro
Sengar et al. (2018)	$Y_{2.99}Pr_{0.01}Al_5O_{12}$@$SiO_2$(300-450 nm)	Protoporphyrin IX (408 nm)	75 nm	1.48 keV	Spectra